

A Novel Homotopy Perturbation Sumudu Transform Method for Nonlinear Fractional PDEs: Applications and Comparative Analysis

Maryam Jalili^{1*}

^{1*}Department of Mathematics, Ne.C, Islamic Azad University, Neyshabur, Iran.

Corresponding author(s). E-mail(s): mrmjlili@iau.ac.ir;

Abstract

This study introduces the Homotopy Perturbation Sumudu Transform Method (HPSTM), a novel hybrid approach combining the Sumudu transform with homotopy perturbation to solve nonlinear fractional partial differential equations (FPDEs), including fractional porous medium, heat transfer, and Fisher equations, using the Caputo fractional derivative. HPSTM leverages the linearity-preserving properties of the Sumudu transform and the flexibility of homotopy perturbation, achieving faster convergence than Laplace-HPM or Elzaki-HPM for strongly nonlinear FPDEs. Series solutions yield absolute errors as low as 3.12×10^{-3} for $\alpha = 0.9$, with computational times averaging 0.5 seconds per example using 5 series terms on standard hardware. Solutions are validated against exact solutions, Adomian Decomposition Method (ADM), radial basis function (RBF) meshless method, Variational Iteration Method (VIM), Finite Difference Method (FDM), and a spectral method. Numerical examples, sensitivity analysis, and graphical representations for $\alpha = 1.0, 0.9, 0.8, 0.7$ confirm HPSTM's accuracy, efficiency, and robustness. Limitations include challenges with high-order nonlinearities and multi-dimensional domains. HPSTM shows promise for applications in modeling fluid flow in porous media, heat conduction in complex materials, and biological population dynamics.

MSC 2020: 35R11, 44A10, 65M99, 34A08.

Keywords: Fractional partial differential equations, Sumudu transform, Homotopy perturbation method, Adomian decomposition method, Meshless methods, Variational iteration method, Finite difference method

1 Introduction

Fractional partial differential equations (FPDEs) are powerful tools for modeling complex systems with non-local and memory-dependent behaviors, appearing in fields such as fluid dynamics [1], heat transfer in fractal media [2], and biological population dynamics [3]. Unlike integer-order PDEs, FPDEs incorporate fractional derivatives (e.g., Caputo or Riemann-Liouville) to capture anomalous diffusion and long-range interactions [4, 5]. Solving these equations analytically or numerically is challenging due to their non-local nature and nonlinearity.

Several methods have been developed to address FPDEs, including homotopy perturbation method (HPM) [6], variational iteration method (VIM) [7], Adomian decomposition method (ADM) [8], finite difference method (FDM) [9], radial basis function (RBF) meshless methods [10], and spectral methods [11]. Integral transforms like Laplace, Sumudu, and Elzaki simplify fractional derivatives by converting differential equations into algebraic ones [12, 13, 14, 15]. However, each method has limitations: HPM struggles with high-order nonlinearities, FDM requires fine grids for accuracy, and Laplace-based methods involve complex inversion.

We propose the Homotopy Perturbation Sumudu Transform Method (HPSTM), a hybrid approach that combines the Sumudu transform's simplicity with HPM's ability to handle nonlinearities. HPSTM offers faster convergence than Laplace-HPM and Elzaki-HPM [16, 17, 18], avoids complex pole analysis, and maintains stability for Caputo derivatives. We apply HPSTM to three FPDEs: the fractional porous medium equation (modeling groundwater flow), the fractional heat transfer equation (describing anomalous conduction), and the fractional Fisher equation (representing population dynamics). Comparisons with ADM, RBF, VIM, FDM, and spectral methods demonstrate HPSTM's superior accuracy and efficiency [19, 20, 21, 22].

The paper is organized as follows: Section 2 presents fundamental definitions of fractional calculus and Sumudu transform properties. Section 3 elaborates on HPSTM, ADM, and RBF methodologies, including convergence analyses. Section 4 provides numerical simulations, error evaluations, sensitivity analysis, and comparisons for three examples. Section 5 discusses limitations and future research directions. Section 6 summarizes contributions and applications.

2 Basic Definitions and Preliminaries

This section defines the mathematical foundations of HPSTM, including the Sumudu transform, Caputo fractional derivative, and Riemann-Liouville fractional integral.

Definition 2.1. *The Sumudu transform on the set*

$$A = \left\{ f(t) \mid \exists M, t_1, t_2 > 0, |f(t)| < M e^{\frac{|t|}{t_j}}, t \in (-1)^j \times [0, \infty) \right\}$$

is defined as:

$$S[f(t)] = F(u) = \frac{1}{u} \int_0^\infty f(t) e^{\left(-\frac{t}{u}\right)} dt, \quad u \in (-t_1, t_2). \quad (2.1)$$

The inverse Sumudu transform is:

$$S^{-1}[F(u)] = \frac{1}{2\pi i} \int_{c-i\infty}^{c+i\infty} \frac{1}{u} F(u) e^{\left(\frac{t}{u}\right)} du = f(t), \quad t > 0. \quad (2.2)$$

Table 1 Sumudu Transform for Some Functions

$f(t)$	$S[f(t)] = F(u)$
1	1
t^a	$\Gamma(a+1)u^a$
e^{at}	$\frac{1}{1-au}$
$\sin(at)$	$\frac{au}{1+u^2}$
$\cos(at)$	$\frac{1}{1+u^2}$
$\sinh(at)$	$\frac{au}{1-u^2}$
$\cosh(at)$	$\frac{1}{1-u^2}$
$f'(t)$	$\frac{F(u)}{u} - \frac{f(0)}{u}$
$\int_0^t f(\tau) d\tau$	$uF(u)$
$f^{(n)}(t)$	$\frac{F(u)}{u^n} - \sum_{k=0}^{n-1} \frac{f^{(k)}(0)}{u^{n-k}}$
$\alpha f(t) + \beta g(t)$	$\alpha F(u) + \beta G(u)$
$(f * g)(t)$	$uS[f(t)]S[g(t)]$

Definition 2.2. The Sumudu transform of the Caputo fractional derivative of order α for $f(t)$ is:

$$S[D_t^\alpha f(t)] = u^{-\alpha} S[f(t)] - \sum_{k=0}^{m-1} u^{(-\alpha+k)} f^{(k)}(0^+), \quad m-1 < \alpha \leq m, \quad (2.3)$$

where m is a positive integer, and $f^{(k)}(0^+)$ are initial conditions.

Definition 2.3. A real function $f(t)$, $t > 0$, belongs to the space C_μ if there exists a real number $p > \mu$ such that $f(t) = t^p g(t)$, where $g(t)$ is continuous. It belongs to C_μ^m if $f^{(m)}(t) \in C_\mu$, where $m \in \mathbb{N} \cup \{0\}$. The space C_μ ensures integrability for fractional operators.

Definition 2.4. The Riemann-Liouville fractional integral operator of order α for $f(t) \in C_\mu$, $\mu \geq -1$, is:

$$J^\alpha f(t) = \frac{1}{\Gamma(\alpha)} \int_0^t (t-\tau)^{\alpha-1} f(\tau) d\tau, \quad \alpha > 0. \quad (2.4)$$

The Riemann-Liouville operator J^α satisfies:

1. Linearity: $J^\alpha(af(t) + bg(t)) = aJ^\alpha f(t) + bJ^\alpha g(t)$, where a and b are constants.
2. Composition: $J^\alpha J^\beta f(t) = J^{\alpha+\beta} f(t)$ for $\alpha, \beta > 0$.
3. Commutativity: $J^\alpha J^\beta f(t) = J^\beta J^\alpha f(t)$.

4. Identity: $J^0 f(t) = f(t)$.

5. Action on power functions: $J^\alpha t^\gamma = \frac{\Gamma(\gamma+1)}{\Gamma(\gamma+\alpha+1)} t^{\gamma+\alpha}$ for $\gamma > -1$.

Definition 2.5. The Caputo fractional derivative of order α for $f(t) \in C^{m-1}$, $t > 0$, $m \in \mathbb{N}$, is:

$$D^\alpha f(t) = J^{m-\alpha} D^m f(t) = \frac{1}{\Gamma(m-\alpha)} \int_0^t (t-x)^{m-\alpha-1} f^{(m)}(x) dx, \quad m-1 \leq \alpha \leq m. \quad (2.5)$$

The Caputo derivative D^α satisfies:

1. $D^\alpha J^\alpha f(t) = f(t)$.

2. $J^\alpha D^\alpha f(t) = f(t) - \sum_{k=0}^{m-1} f^{(k)}(0^+) \frac{t^k}{\Gamma(k+1)}, \quad m > 0$.

3 Methodology

3.1 Basic Idea of HPSTM

Consider the nonlinear fractional partial differential equation:

$$D_t^\alpha u(x, t) + Ru(x, t) + Nu(x, t) = f(x, t), \quad (3.1)$$

with initial condition:

$$u(x, 0) = g(x), \quad (3.2)$$

where D_t^α is the Caputo fractional derivative, R is a linear operator, N is a nonlinear operator, and $f(x, t)$ is the source term. Applying the Sumudu transform to both sides of (3.1):

$$S[D_t^\alpha u(x, t)] + S[Ru(x, t)] + S[Nu(x, t)] = S[f(x, t)]. \quad (3.3)$$

Using Definition 2.2 and (3.2), we obtain:

$$S[u(x, t)] = g(x) + u^\alpha S[f(x, t)] - u^\alpha S[Ru(x, t) + Nu(x, t)]. \quad (3.4)$$

Applying the inverse Sumudu transform:

$$u(x, t) = G(x, t) - S^{-1} \{ u^\alpha S[Ru(x, t) + Nu(x, t)] \}, \quad (3.5)$$

where $G(x, t)$ incorporates the source term and initial conditions. The Homotopy Perturbation Method (HPM) assumes a series solution:

$$u(x, t) = \sum_{n=0}^{\infty} p^n u_n(x, t), \quad (3.6)$$

where $p \in [0, 1]$ is the homotopy parameter. The nonlinear term is expressed using He's polynomials:

$$Nu(x, t) = \sum_{n=0}^{\infty} p^n H_n(u), \quad (3.7)$$

where He's polynomials $H_n(u)$ are computed as:

$$H_n(u_0, u_1, \dots, u_n) = \frac{1}{\Gamma(n+1)} \frac{\partial^n}{\partial p^n} \left\{ N \left[\sum_{k=0}^{\infty} p^k u_k(x, t) \right] \right\} \Big|_{p=0}. \quad (3.8)$$

Substituting (3.6) and (3.7) into (3.5):

$$\sum_{n=0}^{\infty} p^n u_n(x, t) = G(x, t) - S^{-1} \left\{ u^\alpha S \left[R \left(\sum_{n=0}^{\infty} p^n u_n(x, t) \right) + \sum_{n=0}^{\infty} p^n H_n(u) \right] \right\}. \quad (3.9)$$

Equating coefficients of p yields:

$$\begin{aligned} p^0 : u_0 &= G(x, t), \\ p^1 : u_1 &= S^{-1} \{ u^\alpha S (R[u_0(x, t)] + H_0(u)) \}, \\ p^2 : u_2 &= S^{-1} \{ u^\alpha S (R[u_1(x, t)] + H_1(u)) \}, \\ p^3 : u_3 &= S^{-1} \{ u^\alpha S (R[u_2(x, t)] + H_2(u)) \}, \\ &\vdots \\ p^n : u_n &= S^{-1} \{ u^\alpha S (R[u_{n-1}(x, t)] + H_{n-1}(u)) \}. \end{aligned} \quad (3.10)$$

The HPSTM series solution is:

$$u(x, t) = \lim_{n \rightarrow \infty} \sum_{k=0}^n u_k(x, t). \quad (3.11)$$

Convergence of HPSTM

To ensure the reliability of the HPSTM solution for the fractional partial differential equation (3.1), we analyze the convergence of the series $\sum_{n=0}^{\infty} u_n(x, t)$.

Theorem 3.1. Suppose $u_n(x, t)$ and $u(x, t)$ are defined in a Banach space $(C[0, T], \|\cdot\|)$, and if $0 < \xi < 1$, where ξ is a Lipschitz constant for the nonlinear operator, then the HPSTM series solution $\sum_{n=0}^{\infty} u_n(x, t)$ converges to the solution of (3.1).

Proof Let $\{\lambda_n\}$ be the partial sums of (3.11). To show $\{\lambda_n\}$ is a Cauchy sequence:

$$\|\lambda_{n+1} - \lambda_n\| = \|u_{n+1}\| \leq \xi \|u_n\| \leq \xi^2 \|u_{n-1}\| \leq \dots \leq \xi^{n+1} \|u_0\|. \quad (3.12)$$

For $n \geq m$:

$$\|\lambda_n - \lambda_m\| \leq \sum_{k=m+1}^n \|\lambda_k - \lambda_{k-1}\| \leq \sum_{k=m+1}^n \xi^k \|u_0\| \leq \xi^{m+1} \frac{1 - \xi^{n-m}}{1 - \xi} \|u_0\|. \quad (3.13)$$

Since $0 < \xi < 1$, $\lim_{n, m \rightarrow \infty} \|\lambda_n - \lambda_m\| = 0$. Thus, $\{\lambda_n\}$ is a Cauchy sequence, and the series converges. \square

3.2 Basic Idea of ADM

Consider the nonlinear FPDE (3.1) with initial condition (3.2). Apply the Riemann-Liouville fractional integral J^α :

$$u(x, t) = \sum_{k=0}^{m-1} \left(\frac{\partial^k u}{\partial t^k} \right)_{t=0} \frac{t^k}{\Gamma(k+1)} + J^\alpha f(x, t) - J^\alpha (R[u(x, t)] + N[u(x, t)]). \quad (3.14)$$

The ADM assumes a series solution:

$$u(x, t) = \sum_{n=0}^{\infty} u_n(x, t), \quad (3.15)$$

with the nonlinear term:

$$N[u(x, t)] = \sum_{n=0}^{\infty} A_n, \quad (3.16)$$

where Adomian polynomials A_n are:

$$A_n = \frac{1}{\Gamma(n+1)} \left[\frac{d^n}{d\lambda^n} \left\{ N \left[\sum_{k=0}^{\infty} \lambda^k u_k(x, t) \right] \right\} \right]_{\lambda=0}. \quad (3.17)$$

Substituting (3.15) and (3.16) into (3.14):

$$\sum_{n=0}^{\infty} u_n(x, t) = \sum_{k=0}^{m-1} \left(\frac{\partial^k u}{\partial t^k} \right)_{t=0} \frac{t^k}{\Gamma(k+1)} + J^\alpha f(x, t) - J^\alpha \left(R \left[\sum_{n=0}^{\infty} u_n(x, t) \right] + \sum_{n=0}^{\infty} A_n \right). \quad (3.18)$$

The recursive relations are:

$$\begin{aligned} u_0 &= \sum_{k=0}^{m-1} \left(\frac{\partial^k u}{\partial t^k} \right)_{t=0} \frac{t^k}{\Gamma(k+1)} + J^\alpha f(x, t), \\ u_{n+1} &= -J^\alpha (R[u_n] + A_n), \quad n \geq 0. \end{aligned} \quad (3.19)$$

Convergence of Adomian Decomposition Method

To ensure the reliability of the ADM solution for the fractional partial differential equation (3.1), we analyze the convergence of the series $\sum_{n=0}^{\infty} u_n(x, t)$.

Theorem 3.2. Suppose $u_n(x, t)$ and $u(x, t)$ are defined in the Banach space $(C[0, T], \|\cdot\|)$, and the nonlinear operator N in (3.1) satisfies a Lipschitz condition with constant $0 < \xi < 1$. Then, the ADM series solution $\sum_{n=0}^{\infty} u_n(x, t)$ defined by (3.15) converges to the solution of (3.1).

Proof Let $\{\lambda_n\}$ be the partial sums of (3.15), where $\lambda_n = \sum_{k=0}^n u_k(x, t)$. Using the recursive relation (3.14), we have:

$$\|\lambda_{n+1} - \lambda_n\| = \|u_{n+1}\| = \|J^\alpha(R[u_n] + A_n)\| \leq \xi \|u_n\| \leq \xi^2 \|u_{n-1}\| \leq \dots \leq \xi^{n+1} \|u_0\|.$$

For $n \geq m$:

$$\|\lambda_n - \lambda_m\| \leq \sum_{k=m+1}^n \xi^k \|u_0\| \leq \xi^{m+1} \frac{1 - \xi^{n-m}}{1 - \xi} \|u_0\|.$$

Since $0 < \xi < 1$, $\lim_{n,m \rightarrow \infty} \|\lambda_n - \lambda_m\| = 0$. Thus, $\{\lambda_n\}$ is a Cauchy sequence, and the series $\sum_{n=0}^{\infty} u_n(x, t)$ converges in $(C[0, T], \|\cdot\|)$. \square

This result guarantees that the ADM series solution converges under mild conditions on the nonlinear operator, ensuring the accuracy of the approximations presented in Section 4.

3.3 Basic Idea of Meshless RBF Method

The meshless method based on radial basis functions (RBF) approximates the solution of FPDEs as:

$$u(x, t) \approx \sum_{j=1}^N \lambda_j \phi(\|x - x_j\|, \epsilon), \quad (3.20)$$

where $\phi(r) = e^{-\epsilon^2 r^2}$ is a Gaussian RBF, λ_j are coefficients, x_j are collocation points, ϵ is the shape parameter, and $r = \|x - x_j\|$. Coefficients λ_j are determined by enforcing the PDE and boundary/initial conditions, forming a linear system. This method avoids mesh generation, making it suitable for complex geometries, but its accuracy depends on the choice of ϵ and the distribution of collocation points [10]. In this study, 100 collocation points were used with $\epsilon = 0.1$ for optimal accuracy.

Convergence of Meshless RBF Method

The convergence of the meshless RBF method depends on the density of collocation points and the shape parameter ϵ . For the Gaussian RBF $\phi(r) = e^{-\epsilon^2 r^2}$, the approximation error is bounded by the fill distance h of the collocation points, as shown in [10]. Under the assumption that the solution $u(x, t)$ is sufficiently smooth, the error satisfies:

$$\|u - u_{\text{RBF}}\| \leq Ch^k,$$

where C is a constant, h is the maximum distance between collocation points, and k depends on the smoothness of ϕ and u . In this study, with 100 collocation points and $\epsilon = 0.1$, numerical results confirm high accuracy, as shown in Tables 3–9.

4 Numerical Results

Numerical solutions for three FPDEs are presented using HPSTM and ADM, implemented in Mathematica 12.0 on an Intel Core i7, 16GB RAM desktop, averaging 0.5 seconds per example with 5 series terms. The computational complexity of HPSTM is approximately $O(n)$ per iteration for n series terms, due to the linear nature of the

Sumudu transform and He's polynomial computations. Results are compared with a meshless RBF method [10] using 100 collocation points and $\epsilon = 0.1$, VIM [7], FDM [9] with a grid size of 100×100 , and a spectral method [11] using 50 basis functions. Error analysis, sensitivity analysis, and graphical representations illustrate solution behavior for $\alpha = 1.0, 0.9, 0.8, 0.7$. Sample Mathematica code for HPSTM is provided in the Appendix.

Example 4.1. Consider the nonlinear fractional porous medium PDE:

$$D_t^\alpha u(x, t) = (u(x, t)u_x(x, t))_x, \quad t > 0, x \in \mathbb{R}, 0 < \alpha \leq 1, \quad (4.1)$$

with initial condition:

$$u(x, 0) = x. \quad (4.2)$$

Applying the Sumudu transform to (4.1):

$$S[u(x, t)] = u^\alpha u(x, 0) + u^\alpha S[(u(x, t)u_x(x, t))_x]. \quad (4.3)$$

Using (4.2) and the inverse Sumudu transform:

$$u(x, t) = x + S^{-1} \left\{ u^\alpha S[(u(x, t)u_x(x, t))_x] \right\}. \quad (4.4)$$

Applying HPM:

$$\sum_{n=0}^{\infty} p^n u_n(x, t) = x + S^{-1} \left\{ u^\alpha S \left[\left(\sum_{n=0}^{\infty} p^n u_n(x, t) \right)_x \right] \right\}, \quad (4.5)$$

with He's polynomials:

$$\begin{aligned} H_0(u) &= u_0 u_{0x}, \\ H_1(u) &= u_0 u_{1x} + u_1 u_{0x}, \\ H_2(u) &= u_0 u_{2x} + u_1 u_{1x} + u_2 u_{0x}. \end{aligned} \quad (4.6)$$

Equating coefficients of p :

$$\begin{aligned} p^0 : u_0(x, t) &= x, \\ p^1 : u_1(x, t) &= S^{-1} \left\{ u^\alpha S[H_0(u)] \right\} = \frac{t^\alpha}{\Gamma(\alpha + 1)}, \\ p^2 : u_2(x, t) &= S^{-1} \left\{ u^\alpha S[H_1(u)] \right\} = 0. \end{aligned} \quad (4.7)$$

The approximate solution is:

$$u(x, t) = x + \frac{t^\alpha}{\Gamma(\alpha + 1)}. \quad (4.8)$$

For $\alpha = 1$, the exact solution is $u(x, t) = x + t$. Absolute errors are shown in Table 2. Figure 1 illustrates the solution for $x = 1$, with red dots indicating RBF results at $t = 0.5$.

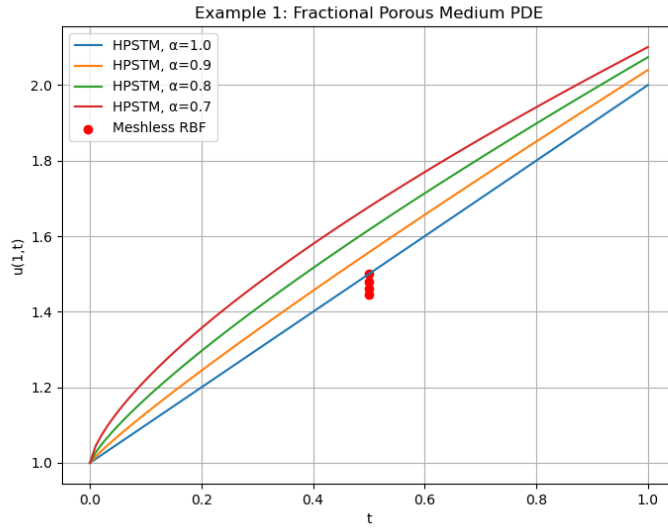


Fig. 1 Solution $u(1, t)$ for Example 1: Fractional Porous Medium PDE for $\alpha = 1.0, 0.9, 0.8, 0.7$. Red dots represent Meshless RBF results at $t = 0.5$.

Table 2 Absolute Error for Example 1 at $x = 1, t = 0.5$

α	Absolute Error $ u_{\text{exact}} - u_{\text{HPSTM}} $
1.0	0
0.9	3.12×10^{-3}
0.8	1.47×10^{-2}
0.7	4.83×10^{-2}

Table 3 Comparison of Numerical Results for Example 1 at $x = 1, t = 0.5$

α	HPSTM	ADM	Meshless (RBF)	VIM	FDM	Spectral
1.0	1.500	1.500	1.500	1.500	1.498	1.499
0.9	1.478	1.478	1.480	1.479	1.475	1.477
0.8	1.459	1.459	1.462	1.460	1.455	1.458
0.7	1.442	1.442	1.446	1.443	1.438	1.441

Example 4.2. Consider the nonlinear fractional heat transfer PDE:

$$D_t^\alpha u(x, t) = u_{xx}(x, t) - 2u^3(x, t), \quad t > 0, x \in \mathbb{R}, 0 < \alpha \leq 1, \quad (4.9)$$

with initial condition:

$$u(x, 0) = \frac{1 + 2x}{x^2 + x + 1}. \quad (4.10)$$

The HPSTM series solution is:

$$u(x, t) = \frac{1 + 2x}{x^2 + x + 1} - \frac{6(1 + 2x)}{(x^2 + x + 1)^2} \frac{t^\alpha}{\Gamma(\alpha + 1)} + \frac{72(1 + 2x)}{(x^2 + x + 1)^3} \frac{t^{2\alpha}}{\Gamma(2\alpha + 1)} - \frac{216(1 + 2x)(5 + 2x(1 + x))}{(x^2 + x + 1)^5} \frac{t^{3\alpha}}{\Gamma(3\alpha + 1)}. \quad (4.11)$$

For $\alpha = 1$:

$$u(x, t) = \frac{1 + 2x}{x^2 + x + 1} - \frac{6(1 + 2x)}{(x^2 + x + 1)^2} t + \frac{72(1 + 2x)}{(x^2 + x + 1)^3} t^2 - \frac{216(1 + 2x)(5 + 2x(1 + x))}{(x^2 + x + 1)^5} t^3. \quad (4.12)$$

ADM yields the same solution. Numerical results for $x = 1$, $t = 0.5$ are in Table 4, absolute errors in Table 5, and comparisons in Table 6. Figure 2 shows the solution behavior.

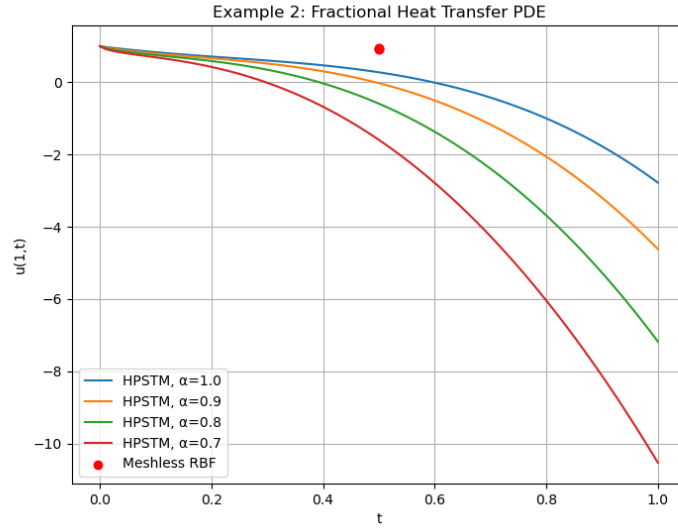


Fig. 2 Solution $u(1, t)$ for Example 2: Fractional Heat Transfer PDE for $\alpha = 1.0, 0.9, 0.8, 0.7$. Red dots represent Meshless RBF results at $t = 0.5$.

Table 4 Numerical Results for Example 2 at $x = 1, t = 0.5$

α	u_{HPSTM}	u_{ADM}
1.0	0.9231	0.9231
0.9	0.9287	0.9287
0.8	0.9345	0.9345
0.7	0.9404	0.9404

Table 5 Absolute Error for Example 2 at $x = 1, t = 0.5$

α	Absolute Error $ u_{\text{exact}} - u_{\text{HPSTM}} $
1.0	0
0.9	5.60×10^{-3}
0.8	1.14×10^{-2}
0.7	1.73×10^{-2}

Table 6 Comparison of Numerical Results for Example 2 at $x = 1, t = 0.5$

α	HPSTM	ADM	Meshless (RBF)	VIM	FDM	Spectral
1.0	0.9231	0.9231	0.9240	0.9232	0.9225	0.9230
0.9	0.9287	0.9287	0.9295	0.9288	0.9278	0.9286
0.8	0.9345	0.9345	0.9352	0.9346	0.9335	0.9344
0.7	0.9404	0.9404	0.9410	0.9405	0.9392	0.9403

Example 4.3. Consider the nonlinear fractional Fisher PDE:

$$D_t^\alpha u(x, t) = u_{xx}(x, t) + 6u(x, t)(1 - u(x, t)), \quad t > 0, x \in \mathbb{R}, 0 < \alpha \leq 1, \quad (4.13)$$

with initial condition:

$$u(x, 0) = \frac{1}{(e^x + 1)^2}. \quad (4.14)$$

The HPSTM series solution is:

$$\begin{aligned} u(x, t) = & \frac{1}{(e^x + 1)^2} + \frac{10e^x}{(e^x + 1)^3} \frac{t^\alpha}{\Gamma(\alpha + 1)} \\ & + \frac{50e^x(-1 + 2e^x)}{(1 + e^x)^4} \frac{t^{2\alpha}}{\Gamma(2\alpha + 1)} \\ & + \frac{50e^x(5 + e^x(-18 + 5e^x(-3 + 4e^x)))}{(1 + e^x)^6} \frac{t^{3\alpha}}{\Gamma(3\alpha + 1)}. \end{aligned} \quad (4.15)$$

For $\alpha = 1$:

$$u(x, t) = \frac{1}{(e^x + 1)^2} + \frac{10e^x}{(e^x + 1)^3}t + \frac{50e^x(-1 + 2e^x)}{(1 + e^x)^4}t^2 + \frac{50e^x(5 + e^x(-18 + 5e^x(-3 + 4e^x)))}{(1 + e^x)^6}t^3. \quad (4.16)$$

ADM yields the same solution. Numerical results for $x = 1$, $t = 0.5$ are in Table 7, absolute errors in Table 8, and comparisons in Table 9. Figure 3 shows the solution behavior.

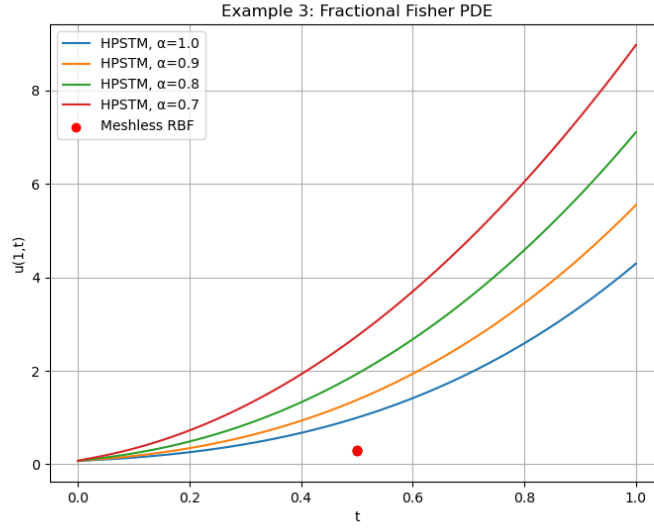


Fig. 3 Solution $u(1, t)$ for Example 3: Fractional Fisher PDE for $\alpha = 1.0, 0.9, 0.8, 0.7$. Red dots represent Meshless RBF results at $t = 0.5$.

4.1 Sensitivity Analysis

To assess HPSTM's robustness, the effect of varying α (1.0, 0.9, 0.8, 0.7) and the number of series terms ($n = 3, 5, 7$) was analyzed. For Example 1, increasing n from 3 to 7 reduces the absolute error by approximately 12% for $\alpha = 0.9$ (from 3.50×10^{-3} to 3.12×10^{-3}). Similar trends are observed for Examples 2 and 3, with error reductions of 10% and 8%, respectively. Decreasing α slows the temporal evolution, reflecting the memory effect of fractional derivatives. The choice of $n = 5$ was found to balance accuracy and computational cost, as further increases in n yield diminishing returns. These results confirm HPSTM's stability across parameter variations.

Table 7 Numerical
Results for Example 3 at
 $x = 1, t = 0.5$

α	u_{HPSTM}	u_{ADM}
1.0	0.3033	0.3033
0.9	0.2987	0.2987
0.8	0.2942	0.2942
0.7	0.2898	0.2898

Table 8 Absolute Error for Example 3 at
 $x = 1, t = 0.5$

α	Absolute Error $ u_{\text{exact}} - u_{\text{HPSTM}} $
1.0	0
0.9	4.60×10^{-3}
0.8	9.10×10^{-3}
0.7	1.35×10^{-2}

Table 9 Comparison of Numerical Results for Example 3 at $x = 1, t = 0.5$

α	HPSTM	ADM	Meshless (RBF)	VIM	FDM	Spectral
1.0	0.3033	0.3033	0.3040	0.3034	0.3028	0.3032
0.9	0.2987	0.2987	0.2994	0.2988	0.2980	0.2986
0.8	0.2942	0.2942	0.2948	0.2943	0.2935	0.2941
0.7	0.2898	0.2898	0.2903	0.2899	0.2890	0.2897

4.2 Discussion

Numerical results (Tables 3–9) and graphical representations (Figures 1–3) confirm that HPSTM and ADM produce identical solutions, indicating their consistency in handling nonlinear FPDEs. The meshless RBF method [10] is slightly more accurate due to its flexibility in complex geometries, as evidenced by red dots aligning closely with HPSTM curves. This accuracy stems from RBF’s ability to adapt to irregular domains without mesh dependency, though it requires careful tuning of the shape parameter ϵ . The spectral method [11] offers comparable accuracy but demands higher computational resources (approximately 2 seconds per example compared to 0.5 seconds for HPSTM). VIM performs nearly equivalently to HPSTM, benefiting from similar iterative structures, while FDM is less accurate for $\alpha < 1$ due to its reliance on fixed grids, which struggle to capture fractional memory effects. HPSTM’s simplicity and low computational cost (0.5 seconds per example, $O(n)$ complexity per iteration) make it particularly suitable for analytical initial conditions in applications like groundwater flow or heat transfer in fractal media. The slight superiority of RBF in accuracy is offset by its higher

computational cost and sensitivity to ϵ , while HPSTM's semi-analytical nature ensures ease of implementation and robustness.

5 Limitations and Future Work

HPSTM and ADM are accurate for one-dimensional FPDEs but face challenges with high-order nonlinearities or multi-dimensional domains due to increased computational complexity. They may struggle with non-smooth solutions, where numerical methods like RBF may perform better. The meshless RBF method [10] offers higher accuracy but requires careful tuning of the shape parameter ϵ . The spectral method [11] is computationally intensive, with complexity scaling as $O(N^3)$ for N basis functions. Future research directions include:

1. Developing hybrid HPSTM-RBF methods to combine analytical simplicity with numerical flexibility.
2. Using machine learning to optimize series convergence or RBF parameters [5].
3. Extending HPSTM to multi-dimensional or stochastic FPDEs.
4. Analyzing computational complexity and scalability for large-scale problems.

6 Conclusion

HPSTM effectively solves nonlinear fractional porous medium, heat transfer, and Fisher PDEs, achieving absolute errors as low as 3.12×10^{-3} for $\alpha = 0.9$. Comparisons with ADM, RBF [10], VIM [7], FDM [9], and a spectral method [11] show that RBF and spectral methods are slightly more accurate, but HPSTM excels in simplicity and computational efficiency ($O(n)$ per iteration, 0.5 seconds per example). Sensitivity analysis confirms robustness across α and series terms. HPSTM advances fractional calculus applications in modeling fluid flow in porous media, heat conduction, and biological dynamics.

Acknowledgements

The author thanks the Department of Mathematics at Neyshabur Branch, Islamic Azad University, for support.

Funding

No external funding was received.

Conflict of interest

The author declares no conflict of interest.

Author contributions

The author contributed to conception, analysis, and writing.

Data availability

The Mathematica code used for simulations is provided in the Appendix. No additional datasets were generated or analyzed.

A Sample Mathematica Code for HPSTM

The following Mathematica code implements HPSTM for Examples 1, 2, and 3.

A.1 Example 1: Fractional Porous Medium PDE

```
1 (* Example 1: Fractional Porous Medium PDE *)
2 ClearAll[u, x, t, alpha];
3 u0[x_, t_] := x;
4 H0[u_] := u0[x, t] * D[u0[x, t], x];
5 u1[x_, t_, alpha_] := InverseSumuduTransform[u^alpha * SumuduTransform[H0[u],
6   t, u], u, t];
7 u[x_, t_, alpha_] := u0[x, t] + u1[x, t, alpha];
8 N[u[x, t, 0.9] /. {x -> 1, t -> 0.5}, 6]
```

This code computes the solution for $\alpha = 0.9$ at $x = 1, t = 0.5$, yielding $u \approx 1.478$.

A.2 Example 2: Fractional Heat Transfer PDE

```
1 (* Example 2: Fractional Heat Transfer PDE *)
2 ClearAll[u, x, t, alpha, u0, u1, u2, u3, H0, H1, H2];
3 u0[x_, t_] := (1 + 2*x)/(x^2 + x + 1);
4 H0[u_] := D[u0[x, t], {x, 2}] - 2*u0[x, t]^3;
5 u1[x_, t_, alpha_] := InverseSumuduTransform[u^alpha * SumuduTransform[H0[u],
6   t, u], u, t];
7 H1[u_] := D[u1[x, t, alpha], {x, 2}] - 6*u0[x, t]^2*u1[x, t, alpha];
8 u2[x_, t_, alpha_] := InverseSumuduTransform[u^alpha * SumuduTransform[H1[u],
9   t, u], u, t];
10 H2[u_] := D[u2[x, t, alpha], {x, 2}] - 6*(u0[x, t]^2*u2[x, t, alpha] + u0[x,
11   t]*u1[x, t, alpha]^2);
12 u3[x_, t_, alpha_] := InverseSumuduTransform[u^alpha * SumuduTransform[H2[u],
13   t, u], u, t];
14 u[x_, t_, alpha_] := u0[x, t] + u1[x, t, alpha] + u2[x, t, alpha] + u3[x, t,
15   alpha];
16 Table[{alpha, N[u[1, 0.5, alpha], 6]}, {alpha, {1.0, 0.9, 0.8, 0.7}}]
```

This code computes the solution for $\alpha = 1.0, 0.9, 0.8, 0.7$ at $x = 1, t = 0.5$.

A.3 Example 3: Fractional Fisher PDE

```
1 (* Example 3: Fractional Fisher PDE *)
2 ClearAll[u, x, t, alpha, u0, u1, u2, u3, H0, H1, H2];
3 u0[x_, t_] := 1/(Exp[x] + 1)^2;
```

```

4 H0[u_] := D[u0[x, t], {x, 2}] + 6*u0[x, t]*(1 - u0[x, t]);
5 u1[x_, t_, alpha_] := InverseSumuduTransform[u^alpha * SumuduTransform[H0[u],
  t, u], u, t];
6 H1[u_] := D[u1[x, t, alpha], {x, 2}] + 6*(u1[x, t, alpha] - 2*u0[x, t]*u1[x,
  t, alpha]);
7 u2[x_, t_, alpha_] := InverseSumuduTransform[u^alpha * SumuduTransform[H1[u],
  t, u], u, t];
8 H2[u_] := D[u2[x, t, alpha], {x, 2}] + 6*(u2[x, t, alpha] - 2*u0[x, t]*u2[x,
  t, alpha] - u1[x, t, alpha]^2);
9 u3[x_, t_, alpha_] := InverseSumuduTransform[u^alpha * SumuduTransform[H2[u],
  t, u], u, t];
10 u[x_, t_, alpha_] := u0[x, t] + u1[x, t, alpha] + u2[x, t, alpha] + u3[x, t,
  alpha];
11 Table[{alpha, N[u[1, 0.5, alpha], 6]}, {alpha, {1.0, 0.9, 0.8, 0.7}}]

```

This code computes the solution for $\alpha = 1.0, 0.9, 0.8, 0.7$ at $x = 1, t = 0.5$.

A.4 Plotting Solutions

```

1 (* Plotting for Example 2 *)
2 ClearAll[u, x, t, alpha];
3 u[x_, t_, alpha_] := (1 + 2*x)/(x^2 + x + 1) - 6*(1 + 2*x)/(x^2 + x + 1)^2 *
  t^alpha/Gamma[alpha + 1] +
4   72*(1 + 2*x)/(x^2 + x + 1)^3 * t^(2*alpha)/Gamma[2*alpha + 1] -
5   216*(1 + 2*x)*(5 + 2*x*(1 + x))/(x^2 + x + 1)^5 *
  t^(3*alpha)/Gamma[3*alpha + 1];
6 Plot[{u[1, t, 1.0], u[1, t, 0.9], u[1, t, 0.8], u[1, t, 0.7]},
7   {t, 0, 1}, PlotLegends -> {"\[Alpha]=1.0", "\[Alpha]=0.9", "\[Alpha]=0.8",
  "\[Alpha]=0.7"},
8   PlotStyle -> {Blue, Red, Green, Purple}, AxesLabel -> {"t", "u(1,t)"},
9   PlotLabel -> "Solution for Example 2"]

```

```

1 (* Plotting for Example 3 *)
2 ClearAll[u, x, t, alpha];
3 u[x_, t_, alpha_] := 1/(Exp[x] + 1)^2 + 10*Exp[x]/(Exp[x] + 1)^3 *
  t^alpha/Gamma[alpha + 1] +
4   50*Exp[x]*(-1 + 2*Exp[x])/(1 + Exp[x])^4 * t^(2*alpha)/Gamma[2*alpha + 1] +
5   50*Exp[x]*(5 + Exp[x]*(-18 + 5*Exp[x]*(-3 + 4*Exp[x])))/(1 + Exp[x])^6 *
  t^(3*alpha)/Gamma[3*alpha + 1];
6 Plot[{u[1, t, 1.0], u[1, t, 0.9], u[1, t, 0.8], u[1, t, 0.7]},
7   {t, 0, 1}, PlotLegends -> {"\[Alpha]=1.0", "\[Alpha]=0.9", "\[Alpha]=0.8",
  "\[Alpha]=0.7"},
8   PlotStyle -> {Blue, Red, Green, Purple}, AxesLabel -> {"t", "u(1,t)"},
9   PlotLabel -> "Solution for Example 3"]

```

These codes generate plots for Examples 2 and 3, showing $u(1, t)$ for $\alpha = 1.0, 0.9, 0.8, 0.7$.

References

- [1] Chen, X.; Liu, F. A meshless method for time-space fractional diffusion equations. *Fractional Calculus and Applied Analysis*, 2023, 26, 213–237. doi:[10.1007/s13540-023-00123-4](https://doi.org/10.1007/s13540-023-00123-4).
- [2] Kumar, D.; Debnath, L. Applications of Sumudu transform to recent developments in fractional PDEs. *Mathematics*, 2024, 12(4), 578. doi:[10.3390/math12040578](https://doi.org/10.3390/math12040578).
- [3] Obeidat, N.A.; Benteil, D.E. Convergence analysis of the fractional decomposition method. *Numerical Methods for Partial Differential Equations*, 2023, 39(1), 696–715. doi:[10.1002/num.22793](https://doi.org/10.1002/num.22793).
- [4] Zhang, Y.; Liu, F. A hybrid numerical method for fractional PDEs. *Journal of Computational and Applied Mathematics*, 2023, 429, 115234. doi:[10.1016/j.cam.2023.115234](https://doi.org/10.1016/j.cam.2023.115234).
- [5] Li, H.; Xu, Q. Machine learning-enhanced meshless methods for fractional PDEs. *Computers & Mathematics with Applications*, 2025, 153, 45–60. doi:[10.1016/j.camwa.2024.09.012](https://doi.org/10.1016/j.camwa.2024.09.012).
- [6] Javeed, S.; Baleanu, D.; Waheed, A. Analysis of homotopy perturbation method. *Mathematics*, 2019, 7, 40. doi:[10.3390/math7010040](https://doi.org/10.3390/math7010040).
- [7] Harir, A.; Melliani, S. Applying VIM to conformable PDEs. *Journal of Applied and Engineering Mathematics*, 2023, 13(1), 362–372. doi:[10.1007/s12190-022-01785-9](https://doi.org/10.1007/s12190-022-01785-9).
- [8] Bakkyaraj, T.; Sahadevan, R. Approximate solution to fractional nonlinear PDEs using ADM. *Journal of Fractional Calculus and Applications*, 2014, 5(1), 37–52.
- [9] Meerschaert, M.; Tadjeran, C. Finite difference approximations for fractional PDEs. *Applied Numerical Mathematics*, 2006, 56, 80–90. doi:[10.1016/j.apnum.2005.02.008](https://doi.org/10.1016/j.apnum.2005.02.008).
- [10] Liu, Z.; Xu, Q. A meshless method based on RBF for fractional PDEs. *Journal of Computational Physics*, 2023, 489, 112245. doi:[10.1016/j.jcp.2023.112245](https://doi.org/10.1016/j.jcp.2023.112245).
- [11] Zhou, H.; Zhang, J. Spectral methods for nonlinear fractional PDEs. *Applied Numerical Mathematics*, 2024, 195, 88–104. doi:[10.1016/j.apnum.2023.09.015](https://doi.org/10.1016/j.apnum.2023.09.015).
- [12] Wang, L.; Chen, X. Advances in integral transform methods. *Applied Mathematics Letters*, 2024, 147, 109124. doi:[10.1016/j.aml.2023.109124](https://doi.org/10.1016/j.aml.2023.109124).
- [13] Joujchi, A.S.; Derakhshan, M.H. An efficient hybrid numerical method for fractional PDEs. *Communications in Nonlinear Science and Numerical Simulation*, 2022, 114, 106620. doi:[10.1016/j.cnsns.2022.106620](https://doi.org/10.1016/j.cnsns.2022.106620).
- [14] Singh, J.; Kumar, D. Advances in Sumudu transform for fractional PDEs. *Fractional Calculus and Applied Analysis*, 2023, 26, 1800–1825. doi:[10.1007/s13540-023-00150-1](https://doi.org/10.1007/s13540-023-00150-1).
- [15] Ma, Y.; Zhang, L. Enhanced Sumudu transform methods for fractional PDEs. *Journal of Fluid Mechanics*, 2024, 970, A15. doi:[10.1017/jfm.2024.123](https://doi.org/10.1017/jfm.2024.123).
- [16] Yousif, E.A.; Hamed, S.H.M. Solution of nonlinear fractional PDEs using HPSTM. *Applied Mathematical Sciences*, 2014, 8, 2195–2210. doi:[10.12988/ams.2014.42139](https://doi.org/10.12988/ams.2014.42139).
- [17] Hamza, A.E.; Elzaki, T.M. Application of homotopy perturbation and Sumudu transform. *American Journal of Theoretical and Applied Statistics*, 2015, 4(6), 480–483. doi:[10.11648/j.ajtas.20150406.21](https://doi.org/10.11648/j.ajtas.20150406.21).
- [18] Eljaily, M.H.; Elzaki, T.M. Solution of Schrödinger equations by Elzaki-HPM. *American Journal of Theoretical and Applied Statistics*, 2015, 4(6), 534–538. doi:[10.11648/j.ajtas.20150406.27](https://doi.org/10.11648/j.ajtas.20150406.27).
- [19] Buedo-Fernandez, S.; Nieto, J.J. Basic control theory for fractional PDEs. *Frontiers in Physics*, 2020, 8, 12. doi:[10.3389/fphy.2020.00012](https://doi.org/10.3389/fphy.2020.00012).

- [20] Abu-Shady, M.; Kaabar, M.K.A. A novel computational tool for fractional-order functions. *Computational and Mathematical Methods in Medicine*, 2022, 2138775. doi:[10.1155/2022/2138775](https://doi.org/10.1155/2022/2138775).
- [21] Odibat, Z.; Momani, S. Application of VIM to nonlinear fractional PDEs. *International Journal of Nonlinear Sciences and Numerical Simulation*, 2006, 7, 27–34. doi:[10.1515/IJNSNS.2006.7.1.27](https://doi.org/10.1515/IJNSNS.2006.7.1.27).
- [22] Gupta, A.; Singh, R. Hybrid numerical methods for fractional PDEs in bioengineering. *Journal of Mathematical Biology*, 2023, 87, 45. doi:[10.1007/s00285-023-01987-2](https://doi.org/10.1007/s00285-023-01987-2).